# Pre-neutron-emission mass distributions for low-energy neutron-induced actinide fission

Xiaojun Sun,* Chenggang Yu, and Ning Wang†
*Department of Physics, Guangxi Normal University, Guilin 541004, People's Republic of China*
(Received 5 October 2011; revised manuscript received 4 January 2012; published 30 January 2012)

According to the driving potential of a fissile system, we propose a phenomenological fission potential for a description of the pre-neutron-emission mass distributions of neutron-induced actinide fission. Based on the nucleus-nucleus potential with the Skyrme energy-density functional, the driving potential of the fissile system is studied considering the deformations of nuclei. The energy dependence of the potential parameters is investigated based on the experimental data for the heights of the peak and valley of the mass distributions. The pre-neutron-emission mass distributions for reactions $^{238}$U$(n,f)$, $^{237}$Np$(n,f)$, $^{235}$U$(n,f)$, $^{232}$Th$(n,f)$, and $^{239}$Pu$(n,f)$ can be reasonably well reproduced. Some predictions for these reactions at unmeasured incident energies are also presented.

DOI: 10.1103/PhysRevC.85.014613 PACS number(s): 24.75.+i, 25.85.Ec, 25.40.−h

## I. INTRODUCTION

Nuclear fission has been a field of very intense study in the past decade [1–7]. Two of the most interesting characteristics of neutron-induced fission are the huge difference of the mass distribution of the fission fragments for different nuclei and the dramatic change of the mass distribution with the variation of the incident energies of the neutron. It is still far from clear how the parent nucleus transforms into a variety of daughter pairs. The highly excited primary fission fragments, whose mass distributions are called pre-neutron-emission mass distributions, are de-excited by the emission of prompt neutrons, and followed by prompt $\gamma$ rays to form the primary fission products. The primary fission products are usually highly neutron rich and unstable, and gradually evolve to the secondary fission products through the emission of delayed neutrons and the radioactive $\beta$ decay. We will focus on the study of the pre-neutron-emission mass distribution of the primary fission fragments in this work. The precise calculation of the pre-neutron-emission mass distributions is of great importance for understanding the fission process and for describing the yields of the fission products.

The measured mass distribution of the fission fragments can be reasonably well reproduced with some empirical approaches or some systematical methods. Liu *et al.* developed systematics of mass distributions for neutron-induced $^{238}$U fission [8] and of independent yields for neutron-induced $^{235}$U fission [9]. They also presented the evaluation data [10] and the adjusted data [11] for several actinides. Katakura [12,13] and Wahl [14] fitted the experimental data for actinide nuclei with three to seven Gaussian functions. Kibkalo's phenomenological model was designed to study the dependence of the mass distribution on the transferred angular momentum, and was later adapted for predictions of fission yields [15]. A new systematics for fragment mass yields of target nuclei from Th to Bk at incident particle energies between 5 and 200 MeV was developed by Gorodisskiy *et al.* through independent fission modes [16]. The mass distributions predicted with the systematical methods mentioned above are generally described by a series of Gaussians, and the model parameters are obtained through fitting the experimental data. However, available experimental data for energy-dependent neutron-induced fission yields, especially the pre-neutron-emission mass distributions, are not sufficient for the development of global systematics, which results in great difficulties for the predictions of the mass distributions at unmeasured energies.

For a microscopic description of the mass distribution of nuclear fission, the precise calculation of the potential-energy surface seems to be required. Unfortunately, the microscopic calculation of the potential-energy surface of a fissile system is very complicated and time consuming. Some phenomenological approaches are still required for the quantitative description of the energy dependence of the mass distribution at present. It is known that the shell and pairing effects play a key role for the fission and quasifission process. It is found that the quasifission mass distribution in fusion reactions leading to the synthesis of super-heavy nuclei can be reasonably well described by the driving potential in the dinuclear system (DNS) model [17,18], since the shell effects of a reaction system are effectively involved in the driving potential via the $Q$ value of the system. It is therefore interesting to investigate the mass distribution of a fissile system based on its driving potential. Because the deformation effect of a nuclear system influences the process of fusion and fission [19], it is expected that the deformations of nuclei play a role for a reliable calculation of the corresponding driving potential.

In this work, we attempt to propose a simplified fission potential with a few well-determined parameters for quantitatively describing the pre-neutron-emission mass distributions of neutron-induced actinide fission by combining the corresponding driving potential of the fissile system. This paper is organized as follows: In Sec. II, we briefly introduce the calculation of the driving potential of a fissile system. In Sec. III, we introduce the fission potential and its parameters. In Sec. IV, the comparisons between the predicted results and the measured data of the pre-neutron-emission mass distributions for the reactions $^{238}$U$(n,f)$, $^{237}$Np$(n,f)$, $^{235}$U$(n,f)$, $^{232}$Th$(n,f)$, and $^{239}$Pu$(n,f)$ are presented. Finally, the summary and discussion is given in Sec. V.

*sxj0212@gxnu.edu.cn
†wangning@gxnu.edu.cn

 

## II. DRIVING POTENTIAL OF A FISSILE SYSTEM

Assuming that a compound nucleus separates into a pair of nuclei in the fission process,

$$(A_{\rm CN}, Z_{\rm CN}) \rightarrow (A_1, Z_1) + (A_2, Z_2), \tag{1}$$

the corresponding $Q$ value of the system can be expressed as

$$Q = E(A_{\rm CN}, Z_{\rm CN}) - E(A_1, Z_1) - E(A_2, Z_2). \tag{2}$$

Here, $E(A_i, Z_i)$ denotes the energy of a nuclear system with mass $A_i$ and charge $Z_i$. For a description of the potential-energy surface of a fissile system around the scission point, the dinuclear system (DNS) concept may be used, omitting the excitation energies of the fission fragments for simplicity. According to the DNS concept, each fission fragment at the scission point retains its individuality in the evolution of the DNS. This is a consequence of the influence of the shell structure of the partner fragments, since the collective kinetic energy of the fission fragments is low around the scission point. Based on the DNS concept, the driving potential of a fissile system is expressed as

$$D = Q + B_0 \tag{3}$$

in this work, where $B_0$ denotes the Coulomb barrier height in the interaction potential between the fragment pair. Also, the interaction potential $V(R)$ at a center-to-center distance $R$ is calculated by using the Skyrme energy-density functional together with the extended Thomas-Fermi (ETF) approximation [20].

Figure 1 shows the driving potential for $^{235}$U$(n, f)$. The solid circles denote the sum of the $Q$ value and the average total kinetic energy $\overline{\rm TKE}$ of fission fragments at an incident energy of 2 MeV. One sees that there exists a valley at ~140 for the mass number of the heavy fission fragments. The open circles denote the calculated driving potential with the deformations of nuclei being taken into account. Here,

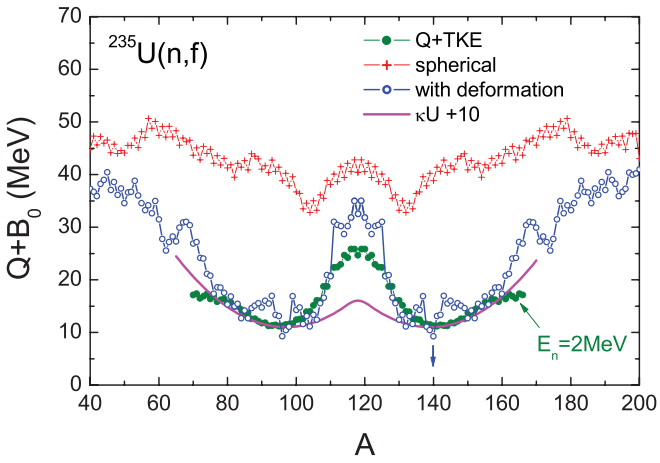


FIG. 1. (Color online) Driving potential for $^{235}$U$(n, f)$. The solid circles denote the sum of the $Q$ value and the average total kinetic energy $\overline{\rm TKE}$ of fission fragments. The crosses and open circles denote the driving potential $D$ without and with the deformations of nuclei being taken into account, respectively. The solid curve denotes the results of $\kappa U + 10$ with $\kappa = 1$ MeV. $U(A)$ denotes the empirical fission potential.

the deformations of nuclei at their ground state are taken from the calculations of the finite-range droplet model [21]. We consider the tip-tip orientation and simultaneously consider the dynamical octupole deformation of fragments (empirically set $|\beta_3| = 0.08$) in the fission process around the scission point, since one obtains a lower Coulomb barrier at the tip-tip orientation. We note that the measured data for $Q + \overline{\rm TKE}$ are roughly reproduced by the calculated driving potential. The crosses denote the results without the deformations of nuclei being taken into account. From the comparison, one learns that the deformations of fragments play an important role for a reasonable description of the fission mass distribution and the total kinetic energy of fragments. The solid curve denotes the result from an empirical fission potential, which will be discussed in the next section.

## III. FISSION POTENTIAL AND ITS PARAMETERS

For a more quantitative description of the mass distribution of primary fission fragments, we further propose an empirical fission potential considering the calculated driving potential. One expects that the pre-neutron-emission mass distribution, i.e., the mass dependence of the primary fission fragments, is strongly dependent on a corresponding fission potential. We assume that the pre-neutron-emission mass distributions of low-energy neutron-induced actinide fission can be approximately described by using a simplified fission potential $U(A)$,

$$P(A) = C \exp[-U(A)], \tag{4}$$

where $C$ is the normalization constant, and the variable $A$ denotes the mass number of the primary fragment. Considering the double-humped mass distributions of low-energy neutron-induced actinide fission, we describe the phenomenological fission potential $U(A)$ by using three harmonic-oscillator functions, i.e.,

$$U(A) = \begin{cases} u_1(A - A_1)^2 & A \leqslant a, \\ -u_0(A - A_0)^2 + R & a \leqslant A \leqslant b, \\ u_2(A - A_2)^2 & A \geqslant b, \end{cases} \tag{5}$$

where $A_1$ and $A_2$ are the positions for the peaks of the light and heavy fragments of the pre-neutron-emission mass distributions, respectively. According to the calculated driving potentials, we find that the valley for the mass number of heavy fragments is located at $A_2 \approx 140$ for neutron-induced actinide fission in general. Therefore, we set $A_2 = 140$ in the calculation for simplicity. We have checked that the calculated mass distribution of fission fragments does not change appreciatively if the value of $A_2$ is slightly changed. $A_0 = A_{\rm CN}/2$ denotes the corresponding position for symmetric fission, where $A_{\rm CN}$ is the mass number of the fissile nucleus. Considering that the fission potential is a smooth function, the coefficients in Eq. (5) can be derived as

$$\begin{aligned} u_0 &= \frac{R}{(A_0 - a)(A_0 - A_1)}, \\ u_1 &= \frac{R}{(A_0 - A_1)(a - A_1)}, \\ u_2 &= \frac{R}{(A_2 - A_0)(A_2 - b)}, \end{aligned} \tag{6}$$

TABLE I. The potential parameters adopted in this work.

| Reaction | $\alpha_1$ | $\beta_1$ | $\alpha_0$ | $\beta_0$ |
|---|---|---|---|---|
| $^{232}$Th$(n,f)$ | 7.0900 | −0.0631 | −0.0656 | 0.0350 |
| $^{235}$U$(n,f)$ | 6.6550 | −0.0952 | −0.0042 | 0.0237 |
| $^{237}$Np$(n,f)$ | 6.4132 | −0.1008 | −0.0113 | 0.0338 |
| $^{238}$U$(n,f)$ | 6.5508 | −0.1090 | −0.0208 | 0.0196 |
| $^{239}$Pu$(n,f)$ | 6.1293 | −0.1517 | 0.0067 | 0.0343 |

with $A_1 = A_{\rm CN} - A_2$ and $b = \dfrac{(A_0 - a)(A_0 - A_1)}{A_2 - A_0} + A_0$. The potential parameters $a$ and $R$ will be discussed later.

The total mass distributions of the binary fission fragments should be normalized to 200%. The normalization constant $C$ can therefore be analytically expressed as

$$C = \frac{200\%}{\int_0^\infty \exp[-U(A)]dA} = \frac{200\%}{I_0 + I_1 + I_2}, \tag{7}$$

with

$$\begin{aligned} I_0 &= \frac{\sqrt{\pi}e^{-R}}{2\sqrt{u_0}}\{\mathrm{erfi}[(A_0 - a)\sqrt{u_0}] + \mathrm{erfi}[(b - A_0)\sqrt{u_0}]\}, \\ I_1 &= \frac{\sqrt{\pi}}{2\sqrt{u_1}}\{\mathrm{erf}[(a - A_1)\sqrt{u_1}\,] + \mathrm{erf}(A_1\sqrt{u_1})\}, \\ I_2 &= \frac{\sqrt{\pi}}{2\sqrt{u_2}}\{1 + \mathrm{erf}[(A_2 - b)\sqrt{u_2}]\}, \end{aligned} \tag{8}$$

where erf$(x)$ and erfi$(x)$ denotes the error function and imaginary error function, respectively. We also assume that $P(A_1) = P(A_2)$, i.e., for the pre-neutron-emission mass distributions, the height of the peak of the light fragments equals that of the heavy fragments. The parameter $a$ can be uniquely determined by the normalization constant $C$ and $P(A_1)$.

The potential parameter $R$ is defined as

$$R = \ln \frac{P(A_1)}{P(A_0)}. \tag{9}$$

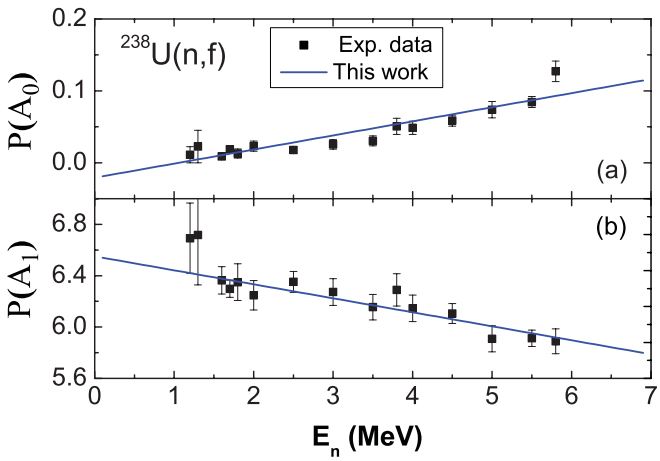


FIG. 2. (Color online) Values of peak $P(A_1)$ and valley $P(A_0)$ of the pre-neutron-emission mass distributions for reaction $^{238}$U$(n,f)$ as a function of incident energy of the neutron. The data are taken from Ref. [22]. The solid lines denote the results in this work.

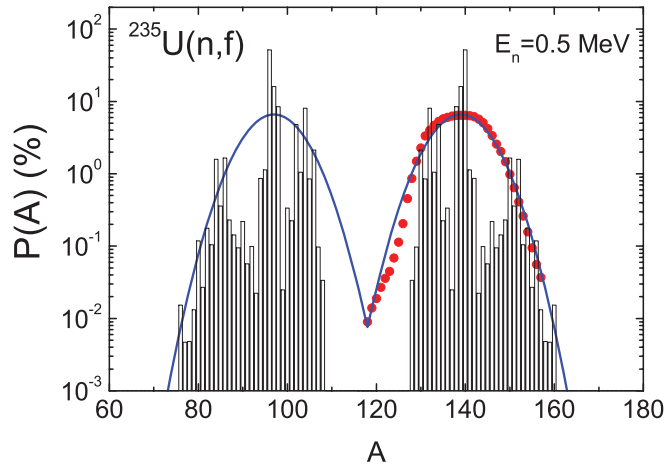


FIG. 3. (Color online) Pre-neutron-emission mass distributions at an incident energy $E_n = 0.5$ MeV for reaction $^{235}$U$(n,f)$. The scattered symbols denote the experimental data, which are taken from Ref. [23]. The solid curve and bars denote the calculated results with the empirical fission potential $U(A)$ and the driving potential, respectively.

We find that the heights of the peak and valley of the mass distributions change linearly with the low incident energies of the neutron in general. The energy dependence of $P(A_0)$ and $P(A_1)$ is written as

$$\begin{aligned} P(A_0) &= \alpha_0 + \beta_0 E_n, \\ P(A_1) &= \alpha_1 + \beta_1 E_n. \end{aligned} \tag{10}$$

Here, $E_n$ denotes the incident energy of the neutron. The parameters $\alpha_0$, $\beta_0$, $\alpha_1$, and $\beta_1$ are finally determined by the experimental data for $P(A_0)$ and $P(A_1)$. The potential parameters for different reaction systems are listed in Table I.

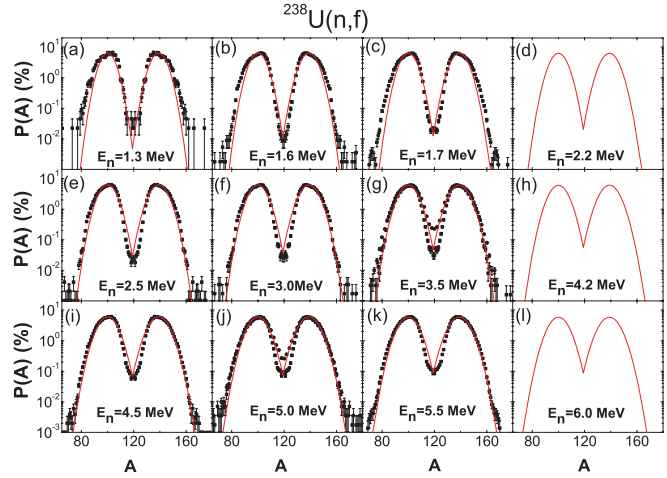


FIG. 4. (Color online) Pre-neutron-emission mass distributions at incident energies from 1.3 to 6 MeV for reaction $^{238}$U$(n,f)$. The scattered symbols denote the experimental data, which are taken from Ref. [22] (squares) and Ref. [24] (circles), respectively. The solid curves denote the calculated results in this work. (d), (h), and (l) show the predicted results at the three unmeasured energies 2.2, 4.2, and 6.0 MeV, respectively.

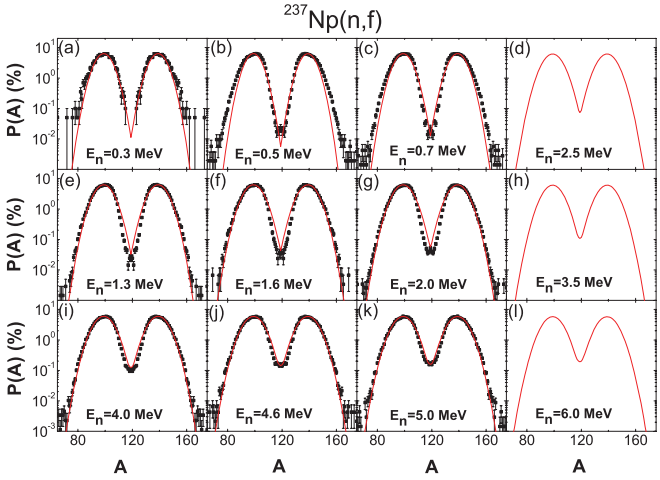


FIG. 5. (Color online) The same as Fig. 4, but for reaction $^{237}\mathrm{Np}(n,f)$ at incident energies from 0.3 to 6.0 MeV. The experimental data (square dots) are taken from Ref. [25].

## IV. RESULTS

In this work, we first investigate the energy dependence of the potential parameters. In Fig. 2, we show the values of $P(A_1)$ and $P(A_0)$ in the pre-neutron-emission mass distributions for the reaction $^{238}\mathrm{U}(n,f)$ as a function of the incident energy of the neutron. One can see that the values of $P(A_1)$ and $P(A_0)$ linearly change with the incident energy in general, which could provide us with some useful information for calculating the pre-neutron-emission mass distributions at unmeasured energies of $E_n \sim$ 1–6 MeV. From the potential parameters listed in Table I, one can see that the values of $\alpha_1$ and $\beta_1$ decrease with the mass number of the fissile nuclei in general. We also note that the potential parameters, such as $A_2$, $P(A_1)$, and $P(A_0)$, are different in different models, and the energy dependence of $A_2$ is weak.

In Fig. 3, we show the comparison of the calculated pre-neutron-emission mass distributions $P(A)$ for $^{235}\mathrm{U}(n,f)$

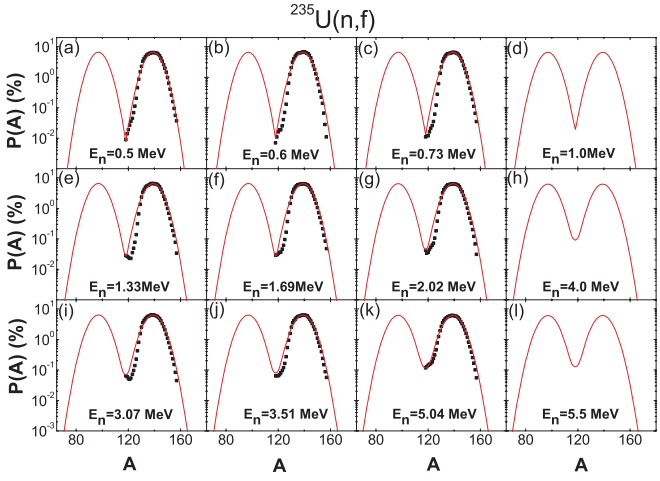


FIG. 6. (Color online) The same as Fig. 4, but for reaction $^{235}\mathrm{U}(n,f)$ at incident energies from 0.5 to 5.5 MeV. The experimental data (square dots) are taken from Ref. [23].

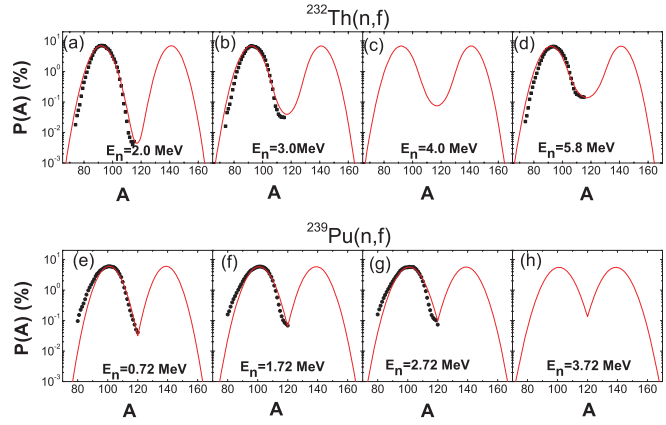


FIG. 7. (Color online) The same as Fig. 4, but (a)–(d) for reaction $^{232}\mathrm{Th}(n,f)$ and (e)–(h) for reaction $^{239}\mathrm{Pu}(n,f)$ at different incident energies. The experimental data are taken from Refs. [26,27].

with the the empirical fission potential and the driving potential, respectively. The solid curve denotes the result with $U(A)$ in Eq. (4). The bars denote the corresponding result with the obtained driving potential in Fig. 1. Here, the mass distribution is roughly estimated by using a formula $P(A) \propto \exp(-D/\kappa)$ based on the obtained driving potential $D$ with $\kappa = 1$ MeV and considering the normalization. One sees that the positions and widths of the peaks for mass distribution can be reasonably well reproduced with the driving potential. The large fluctuation is due to the fact that the temperature dependence of the nuclear structure effect is not considered yet. With the empirical fission potential, the description of the measured mass distribution for the primary fission fragments in $^{235}\mathrm{U}(n,f)$ can be significantly improved.

In Fig. 4, we show the pre-neutron-emission mass distributions $P(A)$ at incident energies from about 1 to 6 MeV for the reaction $^{238}\mathrm{U}(n,f)$. The scattered symbols denote the experimental data, which are taken from Ref. [22] (squares) and from Ref. [24] (circles), respectively. The solid curves denote the calculated results in this work. The potential parameters $\alpha_0$, $\beta_0$, $\alpha_1$, and $\beta_1$ adopted in the calculations are listed in Table I. Figures 5, 6, and 7 show the pre-neutron-emission mass distributions $P(A)$ for the reactions $^{237}\mathrm{Np}(n,f)$, $^{232}\mathrm{Th}(n,f)$, and $^{239}\mathrm{Pu}(n,f)$, respectively. One can see that the experimental data can be reproduced reasonably well, which indicates that the fission potential proposed in this work is reasonable. For some unmeasured energies, we also present the predictions from this approach.

## V. SUMMARY AND DISCUSSION

In this work, we proposed a phenomenological fission potential based on the corresponding driving potential for quantitatively describing the pre-neutron-emission mass distributions of neutron-induced actinide fission at incident energies of the neutron at a few MeV. Based on the nucleus-nucleus potential with the Skyrme energy-density functional, the driving potential of the fissile system is studied, considering

the deformations of nuclei. The measured data for the sum of the $Q$ value and the average total kinetic energy $\overline{\mathrm{TKE}}$ of fission fragments at an incident energy of 2 MeV in $^{235}\mathrm{U}(n,f)$ can be reasonably well reproduced by the calculated driving potential. We also learn that the deformations of nuclei play an important role for a reliable calculation of the driving potential. With a systematic study of the reactions $^{238}\mathrm{U}(n,f)$, $^{237}\mathrm{Np}(n,f)$, $^{235}\mathrm{U}(n,f)$, $^{232}\mathrm{Th}(n,f)$, and $^{239}\mathrm{Pu}(n,f)$, we find that the experimental data of these reactions can be reproduced reasonably well with the proposed fission potential. This investigation is helpful for further describing the yields of the fission products. By combining the radial basis function approach [28], the accuracy and predictive power of the model could be significantly improved. In addition, a more microscopic description of the potential parameters and the temperature dependence of the driving potential should be further investigated. The study of these aspects is underway.

## ACKNOWLEDGMENTS

We thank Min Liu and an anonymous referee for valuable suggestions. This work was supported by the Th-based Molten Salt Reactor Power System of the Strategic Pioneer Science & Technology Projects from the Chinese Academy of Sciences, Defense Industrial Technology Development Program (Grant No. B0120110034) and National Natural Science Foundation of China (Grants No. 10875031, No. 10847004, and No. 11005022).

[1] P. Möller, D. G. Madland, A. J. Sierk, and A. Iwamotoet, Nature (London) **409**, 785 (2001).
[2] P. Möller, A. J. Sierk, and A. Iwamoto, Phys. Rev. Lett. **92**, 072501 (2004).
[3] D. G. Madland, Nucl. Phys. A **772**, 113 (2006).
[4] M. Lammer, IAEA Report No. STI/PUB/1286, 2008 (unpublished), p. 1.
[5] P. Möller, A. J. Sierk, T. Ichikawa, A. Iwamoto, R. Bengtsson, H. Uhrenholt, and S. Åberg, Phys. Rev. C **79**, 064304 (2009).
[6] K. H. Schmidt and B. Jurado, Phys. Rev. Lett. **104**, 212501 (2010).
[7] J. Randrup and P. Möller, Phys. Rev. Lett. **106**, 132503 (2011).
[8] T. J. Liu and Z. J. Sun, IAEA Report No. STI/PUB/1286, 2008 (unpublished), p. 323.
[9] N. C. Shu, T. J. Liu, H. W. Yu, and Y. J. Chen, in *International Conference on Nuclear Data for Science and Technology* (CEA, EDP Sciences, 2008), p. 347.
[10] T. J. Liu, IAEA Report No. STI/PUB/1286, 2008 (unpublished), p. 279.
[11] T. J. Liu, IAEA Report No. STI/PUB/1286, 2008 (unpublished), p. 305.
[12] J. Katakura, IAEA Report No. STI/PUB/1286, 2008 (unpublished), p. 149.
[13] J. Katakura, *A Systematics of Fission Product Mass Yields with 5 Gaussian Functions* (JAERI Research, Nippon Genshiryoku Kenkyujo, 2003).
[14] A. C. Wahl, IAEA Report No. STI/PUB/1286, 2008 (unpublished), p. 117.
[15] Y. V. Kibkalo, IAEA Report No. STI/PUB/1286, 2008 (unpublished), p. 157.
[16] D. M. Gorodisskiy, S. I. Mulgin, A. Y. Rusanov, and S. V. Zhdanov, IAEA Report No. STI/PUB/1286, 2008 (unpublished), p. 183.
[17] G. G. Adamian, N. V. Antonenko, and W. Scheid, Phys. Rev. C **68**, 034601 (2003).
[18] S. A. Kalandarov, G. G. Adamian, N. V. Antonenko, and W. Scheid, Phys. Rev. C **83**, 054611 (2011).
[19] R. K. Gupta, M. Manhas, G. Munzenberg, and W. Greiner, Phys. Rev. C **72**, 014607 (2005).
[20] M. Liu, N. Wang, Z. Li, X. Wu, and E. Zhao, Nucl. Phys. A **768**, 80 (2006).
[21] P. Möller, J. R. Nix, W. D. Myers, and W. J. Swiatecki, At. Data Nucl. Data Tables **59**, 185 (1995).
[22] F. Vivès, F. J. Hambsch, H. Bax, and S. Oberstedt, Nucl. Phys. A **662**, 63 (2000).
[23] P. P. Djachenko *et al.*, Yaderno-Fizicheskie Issledovaniya Report No. 8, 1969 (unpublished).
[24] C. M. Zöller *et al.*, *Seminar on Fission* (Pont d'Oye III, Habay-la-Neuve, Belgium, 1995), p. 56.
[25] F. J. Hambsch, F. Vives, P. Siegler, S. Oberstedt, and J. P. Theobald, Nucl. Phys. A **679**, 3 (2000).
[26] A. I. Sergachev *et al.*, Sov. J. Nucl. Energy **1**, 475 (1968).
[27] N. I. Akimov *et al.*, Yad. Fiz. **13**, 484 (1971) [Sov. J. Nucl. Phys. **13**, 272 (1971)].
[28] N. Wang and M. Liu, Phys. Rev. C **84**, 051303 (2011).